Journal Pre-proof

From mice to rhinos: Whole-organ quantification of 3D mammalian placental structure using correlative multiscale imaging

Davis Laundon, Ella Proudley, Avery Pennington, Aaron Grewal, Philip J. Basford, Orestis L. Katsamenis, James Thompson, Patricia Goggin, Jeanette Norman, Dolapo Adebo, Samuel Kersley, Anandita Umapathy, Lottie Nesbitt, Georgina Constable-Dakeyne, Wendy Irvine, Neil J. Gostling, Pascale Chavatte-Palmer, Bram G. Sengers, Michele C. Darrow, Rohan M. Lewis

PII: S0143-4004(26)00053-6

DOI: https://doi.org/10.1016/j.placenta.2026.02.006

Reference: YPLAC 5429

To appear in: *Placenta*

Received Date: 4 December 2025

Revised Date: 6 January 2026

Accepted Date: 7 February 2026

Please cite this article as: Laundon D, Proudley E, Pennington A, Grewal A, Basford PJ, Katsamenis OL, Thompson J, Goggin P, Norman J, Adebo D, Kersley S, Umapathy A, Nesbitt L, Constable-Dakeyne G, Irvine W, Gostling NJ, Chavatte-Palmer P, Sengers BG, Darrow MC, Lewis RM, From mice to rhinos: Whole-organ quantification of 3D mammalian placental structure using correlative multiscale imaging, *Placenta*, https://doi.org/10.1016/j.placenta.2026.02.006.

From mice to rhinos: Whole-organ quantification of 3D mammalian placental structure using correlative multiscale imaging

Davis Laundon[1,2*], Ella Proudley[1], Avery Pennington[3], Aaron Grewal[4], Philip J Basford[2,4,5], Orestis L Katsamenis[2,5], James Thompson[6], Patricia Goggin[2,6], Jeanette Norman[7], Dolapo Adebo[3], Samuel Kersley[3], Anandita Umapathy[1], Lottie Nesbitt[8], Georgina Constable-Dakeyne[9], Wendy Irvine[9], Neil J Gostling[2,8], Pascale Chavatte-Palmer[10,11], Bram G Sengers[2,4], Michele C Darrow[3], Rohan M Lewis[1,2]

[1]The Institute of Developmental Sciences, Human Development and Health, Faculty of Medicine, University of Southampton, Southampton, SO16 6YD, UK

[2]Institute for Life Sciences, University of Southampton, University Rd, Highfield, Southampton, SO17 1BJ, UK

[3]The Rosalind Franklin Institute, Didcot, OX11 0DE, UK

[4]School of Engineering, Faculty of Engineering and Physical Sciences, University of Southampton, University Road, Southampton, SO17 1BJ, UK

[5]μ-VIS X-Ray Imaging Centre, Faculty of Engineering and Physical Sciences, University of Southampton, Southampton, SO17 1BJ, UK

[6]Biomedical Imaging Unit, Faculty of Medicine, University of Southampton, Southampton, SO16 6YD, UK

[7]Histochemistry Research Facility, Faculty of Medicine, University of Southampton, Southampton, SO16 6YD, UK

[8]School of Biological Sciences, Faculty of Environmental and Life Sciences, University of Southampton, University Rd, Highfield, Southampton, SO17 1BJ, UK

[9]Marwell Wildlife, Thompson's Ln, Colden Common, Winchester, SO21 1JH, UK

[10]Université Paris-Saclay, UVSQ, INRAE, BREED, 78350, Jouy-en-Josas, France

[11]Ecole Nationale Vétérinaire d'Alfort, BREED, 94700, Maisons-Alfort, France

*Address for correspondence:

Davis Laundon

Faculty of Medicine

MP 887, IDS Building, University of Southampton

Southampton General Hospital

Southampton, SO16 6YD, UK

E: D.J.Laundon@soton.ac.uk

Abstract

The mammalian placenta displays extraordinary structural diversity across scales of measurement, yet the quantitative basis and functional consequences of this variation remain poorly understood. Traditional approaches rely on qualitative categories or simple metrics such as length or depth which obscure the complexity of three-dimensional (3D) tissue architecture. Here, we review methods for quantifying whole-organ placental volume, surface area, and vascular organisation, highlighting trade-offs between speed, expense, labour, precision, scalability, destructivity, and specificity. We then demonstrate how correlative multiscale 3D imaging techniques can overcome these limitations, enabling whole-organ quantification across species spanning several orders of magnitude in placental volume—from mouse to rhinoceros. Using integrated workflows that combine X-ray microfocus tomography (microCT), light (H&E histology), and electron (SBF-SEM) microscopy, we generate quantitative structural datasets across spatial scales. In a mouse placenta, correlative 3D X-ray histology (3D-XRH) links histological features directly to their 3D tissue context. In a human placenta, multimodal imaging integrates whole-organ microCT with correlative X-ray and electron microscopy (CXEM) to quantify the total exchange surface area, bridging organ-scale structure and ultrastructural detail. Finally, using placentas from giraffes and rhinos, we show how microCT can be used to quantify the whole organ structure of placentas from even very large mammals, quantifying metrics such as cotyledon volume distribution and blood vessel architecture. Together, these examples illustrate the power of correlative multiscale 3D imaging to resolve mammalian placental structure, bridging cellular and organ-level organisation. This integrative approach provides a unified framework for quantitative comparative placentation, linking structural diversity to physiological function.

KEY WORDS: multiscale, correlative, 3D imaging, microCT, comparative placentation

1. Introduction

Although evolving from a single common ancestor and performing conserved physiological functions, the mammalian placenta exhibits remarkable structural diversity across scales of measurement between species [1-3]. The evolutionary reasons for this structural diversity, and the consequences to physiological function, are poorly understood. At smaller structural levels, mammalian placental interfaces differ in the number of tissue layers separating maternal and fetal circulation and the degree of interdigitation between maternal and fetal tissues. Structural differences in gross placental morphology at the whole organ level, such as volume, exchange surface area, and major blood vessel networks, have received less attention. Variation in gross morphology between mammal species has historically been categorised using a qualitative schema [2, 4, 5]. However, lumping complex biological structures into discrete qualitative categories may obscure important variation. These qualitative categories of gross placental morphology can be ranked as a proxy, from which rates of nutrient transfer can be inferred, but it is not obvious if this is quantitatively true, particularly when integrated across orders of magnitude [1].

Changes in crude placental metrics such as weight and diameter have been associated with disorders such as gestational diabetes [6, 7], pre-eclampsia [8, 9], and growth restriction [10, 11] in human pregnancies. Likewise, changes in placental metrics such as weight and cotyledon number and morphology are indicative of suboptimal reproductive outcomes in livestock species, such as growth restriction [12, 13] or hydrallantois (excessive accumulation of fluid in the allantoic cavity) [14, 15] in horses, sheep, and cows. What is less clear is whether these proxy metrics for available nutrient exchange capacity translate quantitatively to increased surface area or exchange volume and are therefore physiologically meaningful. As with comparative placentation, there exists a trade-off between convenience/ease and accuracy/precision in methods to quantify gross placental structure, and integration of multiple approaches is necessary to fully resolve the interaction of structure and physiological function.

Likewise, the geometry of fetal blood vessel arrangement relative to that of the mother, which is key to understanding nutrient transport and flow, varies between species [1, 16]. Different placental vasculature organisations across mammal species

have also historically been allocated into qualitative categories (e.g. cross-current, counter-current) [2, 17]). In addition to comparative placentation, changes to gross placental vasculature organisation are associated with gestational disorders such as growth restriction and pre-eclampsia in human pregnancies [18, 19], and spontaneous abortion in livestock species [20, 21]. As a branching fractal system, holistic quantitative characterisations of blood vessel networks are particularly challenging to achieve methodologically but are integral to understanding nutrient transport.

Three-dimensional (3D) imaging has been increasingly applied to mammalian placentas and has shed new light on placental structural organisation [1, 16, 22-27]. 3D imaging allows researchers to quantify tissue architecture in its native 3D, both revealing novel structures not resolvable from 2D imaging and structural variation hidden by allocating placental types into qualitative categories [1, 22, 25, 28]. Unlike cruder metrics for gross placental changes, such as weight and diameter proxies, 3D imaging allows precise quantification of exchange regions specifically. Many 3D imaging techniques are also non-destructive of the sample, unlike traditional methods such as conventional histology or resin casting of blood vessels, which permits application of additional modalities downstream in the workflow. Although these benefits come at the cost of the need for specialised imaging equipment and technical training, the potential for 3D imaging techniques in quantifying complex placental structures is vast.

The methodological toolkit available for quantifying gross placental structure is large and diverse (Fig. 1). Each method offers inherent strengths and weaknesses, often representing a trade-off between speed, expense, labour, precision, scalability, destructivity, and specificity [29]. Here, we will review and evaluate the available methods used to quantify volume, surface area, and blood vessel networks in mammalian placentas, with an emphasis on 3D imaging techniques. We then go on to detail how specifically correlative and multiscale 3D imaging workflows can be applied to quantify gross placental structure across orders of magnitude, using primary examples of mammalian placentas (whole mouse, human, giraffe, and rhino placentas, in addition to horse, cow, donkey, and sheep placental samples) from our work.

2. Quantifying whole placental volume

The volume of a placenta differs from placental weight, such as that used to calculate neonate:placental weight ratios for comparison between species [17, 30] and for monitoring pregnancy outcomes clinically [31, 32]. Whereas weight can provide a proxy metric for total energy investment in a placenta relative to a fetus and make inferences about placental efficiency (although this is debatable), the volume represents a placenta's occupation of 3D space. Whereas quantifying exchange structures as a surface area may be most appropriate for sheetlike diffuse placentas, the exchange zone of thick 3D placentas such as discoid placentas (e.g. humans and mice) or placental cotyledons (e.g. sheep and cows) can best be reflected as volumes.

2.1 Volume estimation from geometry & weight, and water displacement

The total volume of a placenta can be estimated by approximating its geometry to a perfect shape. For example, volume can be quickly calculated from one dimensional measurements such as placental length, depth, and width by approximating the placenta to a perfect Euclidean ellipsoid (i.e. volume = 4/3 x π x 0.5 x length x 0.5 x width x 0.5 x depth) or using a convex-concave shell formula [33, 34]. This technique is particularly useful in cases of medical or veterinary *in utero* sonography, where image data are often 2D and *ex vivo* techniques not possible, or where only digital photography is used for placental quantification [35, 36]. However, placentas do not exist as idealised Euclidean shapes and extrapolating 2D metrics from this assumption can only ever be an approximate estimate. As placental mass and volume are tightly correlated ($R \approx 0.96$ [34]), volume can simply be approximated from mass assuming a placental tissue density of 1.05 g/cm^3 as quantified from empirical studies [34, 37, 38]. However, extrapolation of a volume from a known mass tells us nothing about the organisation of the placental structure in 3D space, and it is not known if the 1.05 g/cm^3 density value is conserved across mammal placentas. The water displacement method is an empirical method for placental volume quantification which mitigates against assumption errors in volume extrapolation. In accordance with the Archimedes principle, the placenta is fully submerged in water and the displaced water collected and measured either volumetrically (by volume) or gravimetrically (by weight) [39, 40]. This accounts for the organ's irregular morphology, however the displacement may be inaccurate if air pockets form in or on the placenta and, as above, the raw placental volume does not provide insight into 3D organisation. Also, if not physiologically buffered, water displacement can damage finer tissue structure by osmotic stress

which will reduce the quality of downstream multiscale imaging workflows. This will be less prominent for formalin-fixed tissue, however formalin fixation causes tissue shrinkage which must be considered for downstream quantification.

2.2 Whole placental volume from 3D imaging techniques

3D imaging techniques provide a visualization of how the placenta is organised in 3D space and can be targeted to include only the volume involved in physiological exchange. 3D imaging modalities generate image intensity, whose physical or biological meaning depends on the specific modality. These datasets contain three spatial dimensions (x, y, and z), from which structures of interest can be labelled and quantitatively analysed. Three 3D imaging modalities are specifically suited for whole organ placental volume quantification: sonography, MRI (magnetic resonance imaging), and microCT (micro-computed tomography). Sonography of the placenta [41-44] enables quick, real-time, *in utero* placental imaging which is additionally diagnostic in a clinical or veterinary setting, however the spatial resolution (≈ 0.5-1 mm) and soft tissue contrast is poor compared to other modalities, and motion artefacts are a problem. MRI (magnetic resonance imaging) imaging of the placenta [45, 46] has advantages over sonography in that it offers *in utero* placental images at higher contrast, but acquisition time is much slower and the equipment is more expensive and less portable. microCT imaging of the placenta [16, 47] provides images with better contrast and much higher spatial resolution (≈ 5-50 µm) than either MRI or sonography, however it can only be applied *ex vivo* due to the risks of ionizing radiation on a developing fetus (in clinical settings) and, due to the trade-off between spatial resolution and overall field of view [24], can typically only be applied to whole placentas from small species like rodents. This trade-off makes other higher resolution 3D imaging modalities applied to the placenta, such as confocal fluorescence [23, 48, 49] or volume electron microscopy [1, 22, 24, 25], pragmatically inappropriate for whole organ volume quantification and can only be used for subregions.

Synchrotron-based X-ray computed tomography (sCT) techniques can provide faster imaging, at higher resolution as compared to off-synchrotron microCT imaging, though at the expense of working fully *ex vivo* [50, 51]. Until recently, sCT was limited to small samples only millimetres in diameter, but provided sub-micron resolution, sufficient to image biopsies of human placenta and resolve key features [52]. With the

recent upgrade of the European Synchrotron Radiation Facility to an Extremely Brilliant Source, a new technique called Hierarchical Phase Contrast Tomography (HiP-CT) has become available enabling non-destructive scans of whole human organs with hierarchically increasing resolution (25 µm – 2 µm) [53], resulting in the first HiP-CT scans of whole human placenta in 2025 [54] and highlighting the need for robust, non-manual approaches to segmentation and quantification now that larger, more complex imaging is possible.

3. Quantifying whole placental surface area

Although in discoid and cotyledonary placentas the total exchange region can be best expressed as a volume, actual physiological exchange occurs across biological surfaces like villi or a labyrinth. Therefore, the total available surface area for physiological exchange within gross placental volume must be quantified if these numbers are to be biologically meaningful. For sheet-like diffuse placentas, such as those in horses, rhinos, and pigs, the total exchange region can be best expressed as a surface area, which is further amplified by finer placental structures such as villi and microvilli.

3.1 Surface area estimation from diameter, 2D area, shape, and stereology

As with volume, the surface area of a placenta can be approximated by assuming the organ to be a perfect shape, such as an ellipsoid, and extrapolating from measurements such as diameter [55, 56]. However, only part of the total surface area of a placenta will be involved in physiological exchange and, in discoid and cotyledonary placentas, most of the surface area for exchange is found within the depth of the placenta. The exchange surface can be represented by approximating the placental area to be a 2D shape, such as by segmenting the chorionic plate from digital photographs. This 2D area can only serve as a metric for placental size, however analysis of its geometry can be informative in quantifying placental shape variation beyond allocating placentas into qualitative categories such as ‘oval’, ‘round’, ‘star’, and ‘multi-lobed’ [57, 58]. For diffuse placentas, the total exchange surface area can be represented as a 2D area and, for animals like horses and pigs, the total surface area can be quantified by placing the placenta flat under a clear acrylic marked with regular grids (1-10 cm) [59, 60]. The placental surface area can be calculated by

point counting grids or segmenting a scaled digital photo and doubling the exposed area to account for both sides of the organ.

3.2. Whole placental surface area from 2D and 3D imaging

By far the most widespread imaging-centred approach used to quantify placental surface area across whole organs has been stereology. Stereology is the umbrella term for mathematical and statistical methods used to quantify 3D biological structure from 2D images of tissue subsamples [61, 62] in accordance with the Cavalieri principle. In placental research, stereological approaches have been applied to images from both optical [14, 59, 63-65] and electron [60, 66-69] microscopy, and to quantify placental structures from humans [63, 64], mice [65, 70], and livestock species [14, 59, 71]. As stereology calculates 3D structural information from 2D images, which can be subject to biases in tissue orientation and subsampling, errors in tissue sampling can compound to prejudice quantitation [61]. Stereological sampling also has limitations in that it is laborious, wax tissue sections can become physically distorted, and it is destructive to the tissue. However, when detailed protocols for unbiased systematic random selection for tissue sampling [72], high replication, and image analysis are followed, stereology can provide accurate calculations for 3D placental surfaces areas cheaply and effectively [61, 62]. 3D imaging techniques, both *in utero* and *ex vivo*, are largely as above for volume, quantifying surface area from surface meshes generated from image segmentation. High resolution 3D imaging techniques are advantageous for surface area quantification as they can specifically resolve internal exchange regions, such as the labyrinthine zone of the mouse placenta with contrast-enhanced microCT [47], and branching structures which are inaccurately resolved from 2D imaging alone, such as human placental villi [64, 73].

4. Quantifying whole placental blood vessel networks

Placental blood vessel networks are particularly challenging to quantify methodologically, due to their fractal branching morphology. Accurate quantification of placental networks is however necessary to model nutrient transport and compare ‘efficiency’ variation between species [1, 17, 48, 52, 74-76].

4.1 Blood vessels from 2D and 3D imaging

Major chorionic vessels can be approximated in 2D and traced from digital photographs for larger species, such as humans [77] and horses [20]. The tracings can then be quantified for 2D metrics such as fractality by the boxing counting method [78, 79]. This method is quicker and cheaper than 3D imaging but is limited to the largest visible vessels and cannot account for 3D structure. Likewise, physiologically meaningful placental vascularisation metrics (e.g. vessel volume density, capillary diameter) can be derived from 2D stereology [12, 70, 80], particularly if sections are stained with a vessel-specific marker such as von Willebrand Factor, but these do not account for 3D branching morphometry and arrangement. Placental angiography is an umbrella term for 2D or 3D biomedical imaging techniques focused on resolving placental blood vessels. Vessels are typically labelled with an intravenous contrast-enhancing agent (e.g. those containing iodine, barium, or gadolinium, although imaging can be without contrasting agents [43]) using either radiography, MRI or sonography [43, 81, 82]. Angiography using non-ionizing imaging sources can be applied to placentas *in utero* to assess developmental metrics such as the vascularization flow index [43, 83], however high-resolution vessel geometry is not captured. The gold standard of quantifying placental blood vessel architecture in 3D is corrosion casting followed by microCT imaging [74, 75]. This approach involves cannulating major placental vessels *ex vivo* and perfusing the vasculature with a polymer resin (such as methyl-methacrylate), setting the polymer solid, and corroding the surrounding tissue with a highly alkaline solvent such as potassium hydroxide. The resulting vessel cast can be imaged in 3D by microCT at high resolution (~1-10 µm in XYZ) and the full architecture skeletonised and quantified for complex branching morphometrics such as branching angles, Strahler order, and tortuosity [74, 84]. This method is, however, laborious, involves hazardous reagents, and is totally destructive to the placenta.

5. Correlative multiscale 3D imaging of whole placentas

When selecting a 3D imaging technique for your sample there are pragmatic trade-offs that must be considered, such as the inverse trade-off between spatial resolution and field of view, or sample preparation methods and fluorescence quenching [24, 85, 86]. Correlative imaging workflows (the application of different imaging modalities to

the same sample [85]) can mitigate against the trade-offs and exploit the benefits of individual imaging techniques, making them powerful tools for resolving multiscale structures [1, 26]. Advanced imaging workflows have the benefit of being high resolution, region-specific, precise, and typically non-destructive, however this comes at the cost of greater expense, the need for specialised equipment, and a longer project time than individual imaging techniques.

5.1 Correlative three-dimensional X-ray histology (3D-XRH) of small mammal placentas (whole mouse placenta)

Correlative three-dimensional X-ray histology (3D-XRH) is an imaging technique where formalin-fixed paraffin-embedded (FFPE) tissue blocks are scanned in 3D by microCT prior to destructive sectioning and staining [26, 87, 88]. This generates a 3D volume of the tissue architecture prior to sectioning, which can be both structurally quantified and used to guide region selection for histological sectioning. As the FFPE tissue is processed identically to standard histological sectioning, the sample can be stained as per normal for either hematoxylin and eosin (H&E) or immunolabelling approaches [26], and applied to historic samples. These 2D labelled images can then be correlated back into the 3D image volume to place them in the context of the total tissue architecture, or they can be used to guide segmentation (structure labelling) of the microCT volume. We have previously demonstrated the applicability of 3D-XRH to quantifying mammalian placental structure [26], however the maximum tissue size for 3D-XRH is typically < 1-10 cm, so it is mostly applied to placental samples as opposed to whole organs. 3D-XRH is however a powerful tool for quantifying the whole-organ structure of smaller placentas such as from mice, where whole-width histology sections are well characterised [70, 89]. Figure 2 outlines an example of an E18.5 mouse placenta (total volume 28.8 mm^3) where 3D-XRH is used to quantify the 3D volume and placement of the labyrinthine zone (19.7 mm^3, 68.5% total volume) from an FFPE block, with correlative H&E sections to identify and ground-truth regions in the microCT volume. (The methodology underpinning Figs. 2-6 can be found in *Supplementary Methods.* All segmentation was conducted semi-manually as in [24] using Microscopy Image Browser [90]).

5.2 Multimodal 3D imaging to achieve an integrated multiscale surface area (whole human placenta)

For larger placentas, multiscale quantification can be achieved by applying higher resolution 3D imaging techniques to subsamples from the whole organ. Multiscale imaging of the same sample allows quantification of structures across scales, which can be integrated into a holistic placental 'morphome', defined as the sum of an organ's structural components [1, 91, 92]. Multiscale imaging workflows applied to the human placenta have proven to be powerful tools in quantifying all levels of structure [25, 54, 93]. In Figure 3, we outline an example of this approach to quantify the integrated total exchange surface area of a whole human placenta using multimodal multiscale 3D imaging [1]. The whole organ structure here was imaged on a formalin-fixed iodine-stained term placenta by microCT using a walk-in diondo d5 system, as we have previously detailed for the imaging of an entire horse placenta [16], giving a total placental volume of 457,794 mm^3. Whole width sections were randomly sampled (using a grid system and random number generator) into FFPE blocks, sectioned, and H&E stained for point counting of placental regions, to show that 73.5% of the placental volume was the villous exchange region (the region of the placental organ involved in physiological exchange (intervillous space + chorionic villi) excluding chorionic plate, decidua, and placental septa), giving a total exchange volume of 336,277 mm^3. Prior to formalin fixation, villous tissue (3-5 mm) was subsampled by biopsy needle from the whole placenta immediately after collection and glutaraldehyde fixed to preserve fine structures. Villi were heavy metal stained, and resin embedded for correlative X-ray and electron microscopy (CXEM), a powerful tool for multiscale tissue imaging [94-96], as we have detailed for placental tissue previously [24, 25]. Resin villous blocks were scanned by microCT in a Nikon custom 'Med-X' system to quantify villous surface area per unit volume (14.6 ± 1.1 mm^{-1}). Finally, subregions of the villous resin blocks were excised and mounted for serial block face scanning electron microscopy (SBF-SEM) [97, 98], a 3D electron microscopy technique, to quantify the surface area amplification factor of syncytiotrophoblast microvilli (4.9 ± 1 fold), giving a total integrated surface area of 24.06 m^2. Adjusting for the surface tissue shrinkage factor from FFPE processing of 60.9%, this gives a surface area of 61.5 m^2, comparable to the ~68 m^2 given from stereological approaches [66, 99]. For the 3.95 kg neonate, this equates to 15.6 $m^2\,kg^{-1}$, which can be systematically compared between species.

5.3 Whole-organ microCT imaging of large mammal placentas (whole giraffe and rhino placentas)

The scale of the walk-in diondo d5 microCT system enables the scanning of whole large mammal placentas that are otherwise very challenging to image in 3D [16]. The giraffe placenta is a cotyledonary placenta where physiological exchange with the mother occurs through discrete units called cotyledons [100]. Full 3D imaging of an entire term giraffe placenta (Fig. 4A-F) (total microCT volume = 3,600 cm^3) enables the quantification of cotyledon volume (mean ± SD = 12.0 ± 9.1 cm^3) and distribution (Fig. 4F). Whole-organ quantification of multiple entire giraffe placentas (Fig. 4G-I) shows that that cotyledon size distribution is a right-skewed histogram (Fig. 4H) (skewness = 1.9, kurtosis = 8.5) with most cotyledons of a small to moderate size skewed by a few large outlier cotyledons. Unlike dissecting the cotyledons to measure size by wet weight, whole-organ microCT is non-destructive and the large cotyledons can be located *in situ* to the 3D tissue architecture, on the pregnant horn (Fig. 4F). Cotyledons on the non-pregnant horn are generally smaller than those on the pregnant horn, with the difference being greater for the pre-term placenta (normalised delta Δ = -0.74) than the term placentas (Δ = -0.37 & -0.34). As with the human placenta, subsamples of the whole giraffe placenta can be further processed for downstream correlative multiscale imaging approaches, such as to resolve the long unbranched villi in giraffe placentas from FFPE & CXEM imaging (Fig. 4J-K) and identify trophoblast protrusions in SBF-SEM (Fig. 4L) (perimeter:area ratio = 0.22 μm^{-1} [25]). Indeed, systematic comparison of placental villous tissue between mammal species 3D imaged by CXEM microCT (Fig. 5) reveals remarkable structural variation in villous morphology -both quantitative and qualitative - which is otherwise hidden by a single qualitative 'villous placenta' category and not easily discernible from 2D histological sectioning. We have also previously used 3D imaging to show multiscale structural adaptations in human and equid placental villi consistent with materno-fetal conflict, which are otherwise hidden by a single qualitative category [25].

Likewise, we imaged an entire diffuse rhinoceros placenta (Fig. 6). From the reconstructed placenta (Fig. 6B) (total volume = 5,596 cm^3) we could segment out the blood vessel network at the whole organ level (total volume = 1,135 cm^3) down to a minimum diameter of ~ 2 mm (Fig. 6C-D) [16], identifying arterial and venous portions (Fig. 6C) and resolving the vasculature into its individual vessels (Fig. 6D). Skeletonization of 3D blood vessel networks in the placental horns allowed full quantification of its branching architecture (total length = 8,478 cm, total number of

branches = 1,857). Considering the whole rhino and giraffe placentas (Figs. 5&6), and the whole horse placenta from our previous work [16], vasculature is generally more branched in the pregnant than the nonpregnant horn (Fig. 6E).

Imaging the whole-placenta vascular network allows us to model network parameters like flow resistance. Computational modelling of flow in the actual 3D blood vessel network (Fig. 6F) showed a higher network resistance in the pregnant horn artery (12.3×10^5 Pa s/m^3) than in the non-pregnant horn (3.5×10^5 Pa s/m^3), with the latter value similar to the overall vein resistance (3.7×10^5 Pa s/m^3). Relative resistance decreased rapidly as the network branched out. Flow resistance is sensitive to diameter and vessel dilation will be different in fixed tissue (where the diameter is smaller from tissue shrinkage and resistance higher) to *in vivo*. This may explain the relatively sharp drop in pressure at the inlet of the pregnant horn. However, it should be noted that current simulations include only the larger blood vessels that could be resolved at this scale, while most of the physiological resistance occurs in the arterioles. In larger studies this placental resistance could be related to fetal growth or used to compare between groups or species.

6. Conclusion

The placenta is arguably the most structurally diverse organ in mammals, the reasons for which are not well understood. There exists a vast methodological toolkit for quantifying whole organ placental structure, each with trade-offs. Here, we demonstrated the potential of correlative multiscale imaging workflows to quantify mammalian placental structure across all magnitudes, providing integrated structural measurements and mitigating against the trade-offs of individual imaging modalities. Using examples from mouse to rhino placentas, we show how different workflows can be applied to quantify comparative metrics for species across orders of magnitude (160,000-fold change in volume). Further application of advanced imaging technologies – such as synchrotron imaging, X-ray phase-contrast tomography, and correlative fluorescence techniques – will provide exciting new insights in the future to resolving mammalian placental diversity.

DATA ACCESSIBILITY

All image datasets and corresponding labels associated with this publication are freely available for download at Bioimage Archive accession S-BIAD2433 under license CC BY 4.0 https://www.ebi.ac.uk/biostudies/bioimages/studies/S-BIAD2433

Acknowledgements

This work was funded by the BBSRC grant number BB/Y005953/1. Equipment in the Biomedical Imaging Unit was supported by grant no. MR/L012626/1 Southampton Imaging under MRC UKRMP Funding. The authors acknowledge the µ-VIS X-ray Imaging Centre at the University of Southampton for the provision of the X-ray tomographic imaging facilities. This research used equipment purchased by the National Research Facility for Lab X-ray CT (NXCT) through EPSRC grant EP/T02593X/1. The XRH facility used in this research was launched by the Wellcome trust 'Foundations for routine 3D X-ray histology', grant 212940/Z/18/Z. The Med-X scanner used for this research was developed via the Wellcome trust 'Development of micro-computed tomography (µCT) for enhanced diagnosis and prognosis in interstitial lung diseases (ILD)' grant WT109682MA.

Figures

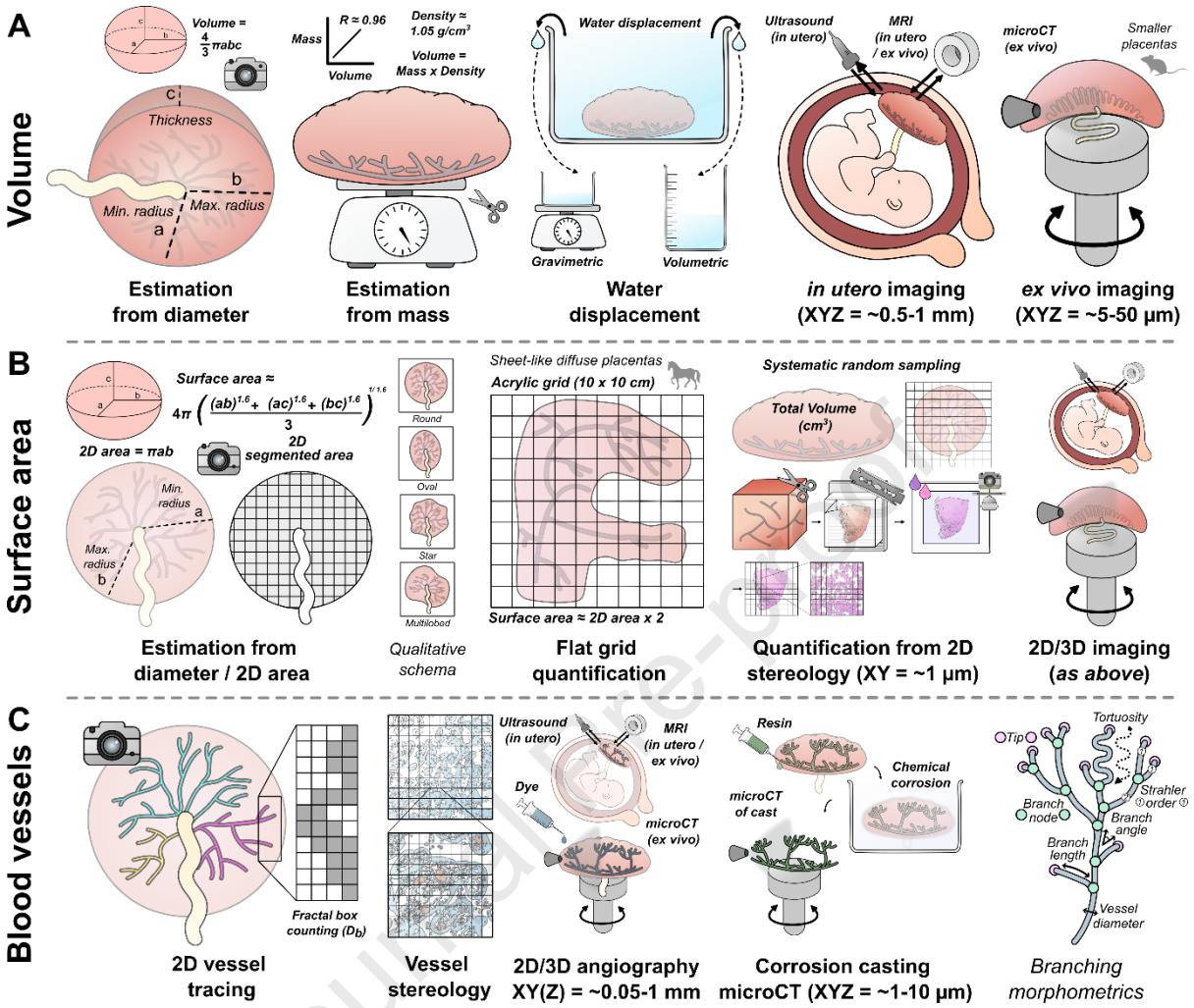

Figure 1 – There is a suite of tools to quantify placental structure at the whole organ level, but each comes with trade-offs. Diagrammatic representation of methodological approaches to quantify (A) volume, (B) surface area, and (C) blood vessel networks in mammalian placentas.

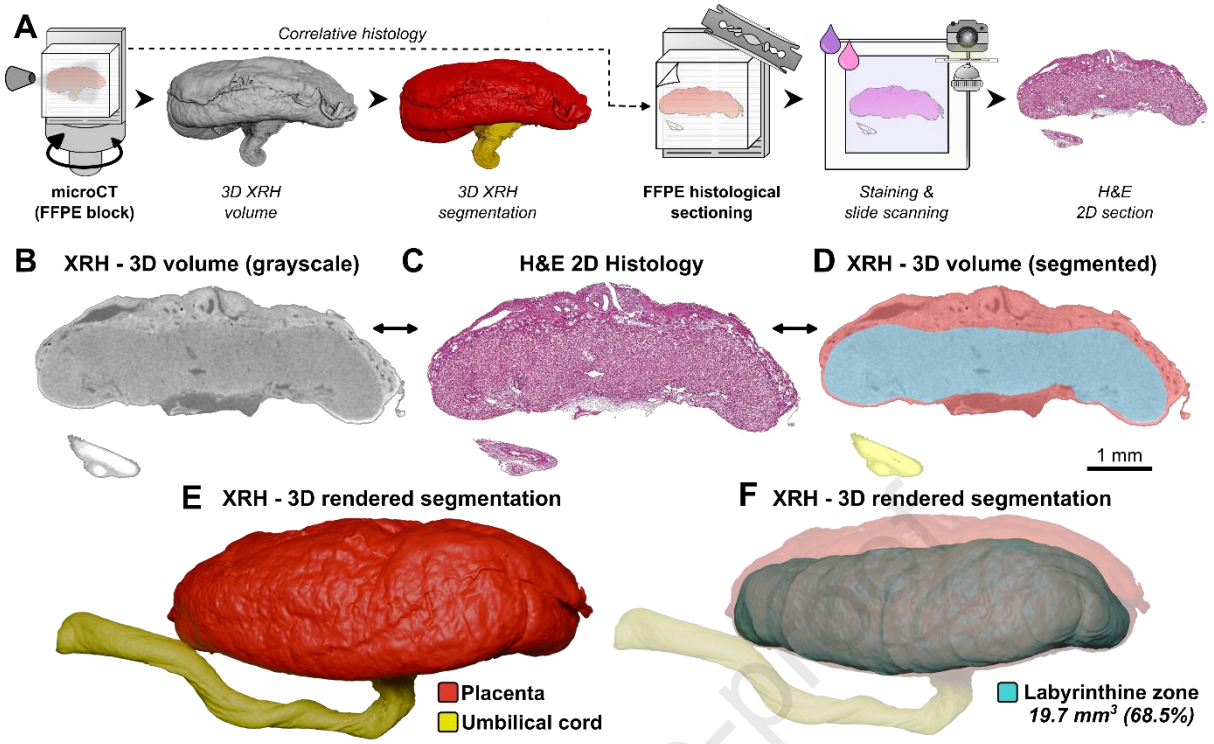

437

438 **Figure 2 - Correlative three-dimensional X-ray histology (3D-XRH) of a whole**
439 **E18.5 mouse placenta.** (A) Diagrammatic representation of the 3D-XRH workflow
440 used to image the whole mouse placenta shown in B-F. (B-D) 3D-XRH generates both
441 a 3D volume of the embedded placenta by non-destructive microCT (B) and correlative
442 2D histology sections (C) which can be used to ground-truth and inform segmentation
443 of the microCT volume (D). (E-F) When reconstructed in 3D, the segmented microCT
444 volume can be used to visualize organ morphology (E) and quantify the volume of
445 specific exchange regions, such as the labyrinthine zone (F).

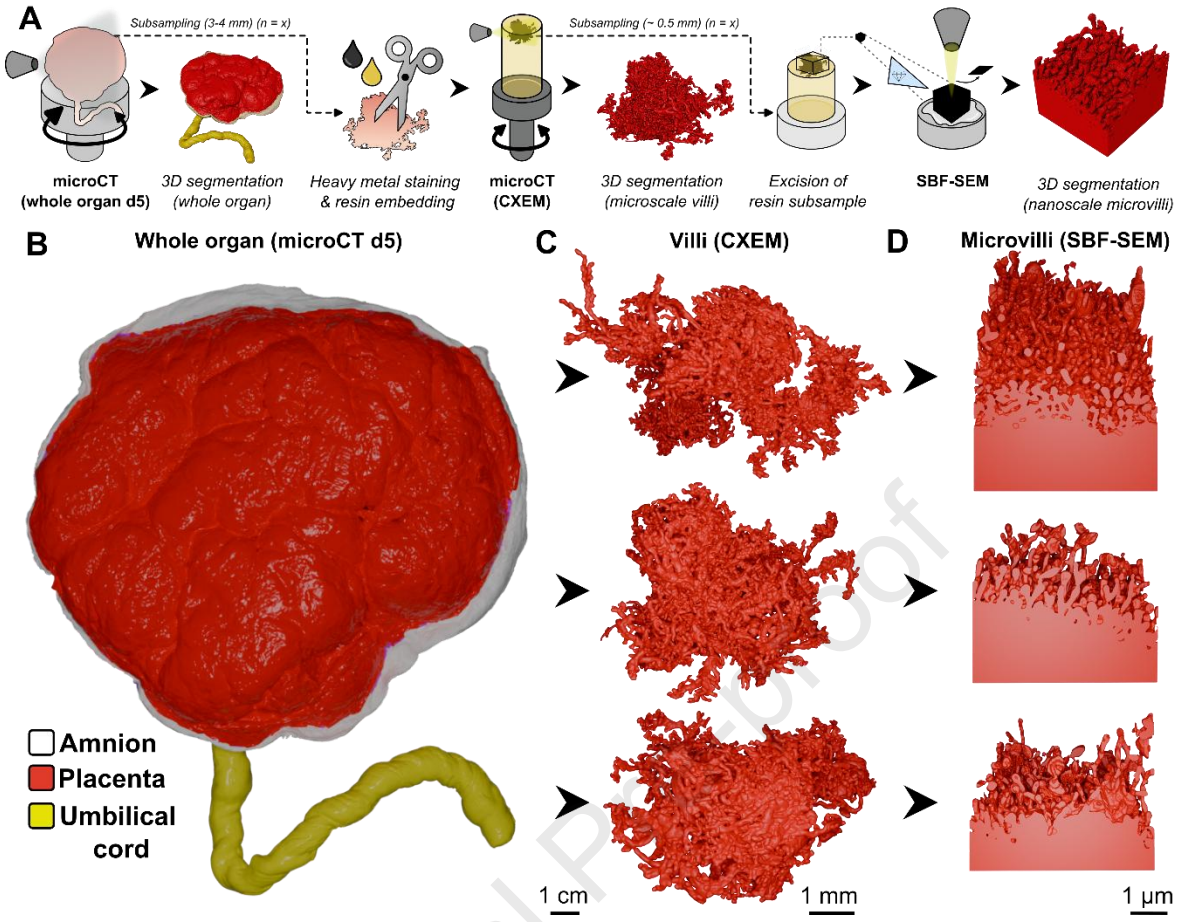

Figure 3 - Multimodal 3D imaging of the integrated multiscale surface area of a human placenta. (A) Diagrammatic representation of the multimodal, multiscale workflow used to image the human placenta shown in B-D. (B) The whole placental volume is imaged by whole-organ microCT in a diondo d5 walk-in system. (C-D) Villus subsamples are processed as if for electron microscopy for CXEM, where the villus surface area is quantified by microCT imaging (C) and a subregion of the trophoblast microvilli surface area amplification factor quantified by SBF-SEM (D). This multimodal multiscale surface area allows the quantification of total integrated surface area in this human placenta.

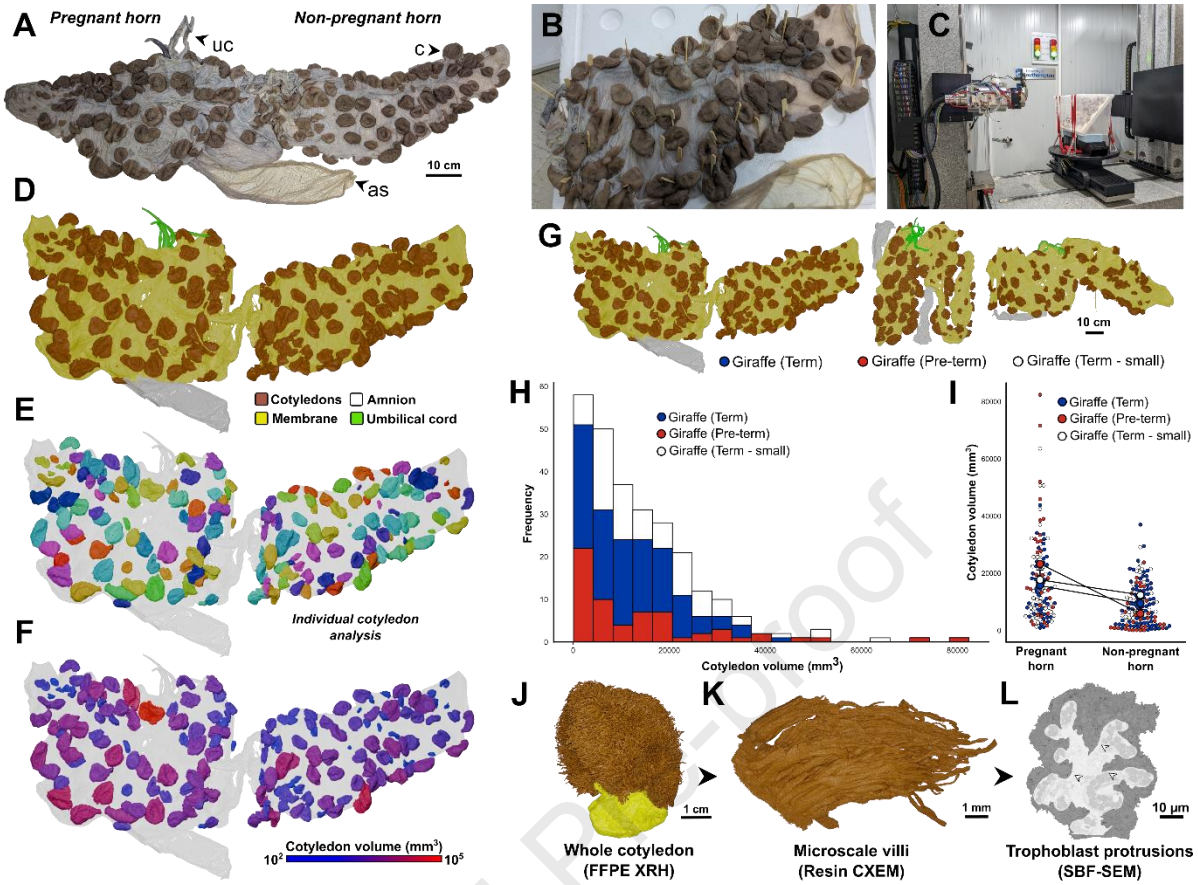

Figure 4 – Whole-organ microCT cotyledon analysis of the giraffe placenta. (A-C) Whole-organ microCT is normally not possible for medium to large mammal placentas, but the diondo d5 walk-in system can fully image in 3D the placenta of even the largest hoofed mammal species. (A) An entire term giraffe placenta was mounted to both sides of a polystyrene board with plastic toothpicks (B) and imaged inside a diondo d5 walk-in microCT system (C) as = amniotic sac, c = cotyledons, uc = umbilical cord. (D-F) Full 3D reconstruction of the whole giraffe placenta in (A) showing major components (D), individual disconnected cotyledons (E), and cotyledons false coloured by size (F). (G-I) Three giraffe placentas were quantitatively imaged in 3D (G), showing a right-skewed distribution of cotyledons sizes (H) and larger cotyledons on the pregnant horn than non-pregnant horn (I). These cotyledon distributions are for the examples presented here and further replication is needed to confirm these preliminary trends. (J-L) The same correlative 3D-XRH (J) and multimodal multiscale CXEM workflows (K-L) from Fig. 3A and Fig. 4A applied to giraffe placental villi, showing the architecture of long unbranched villi (J-K) and trophoblast protrusions (arrowheads) (L).

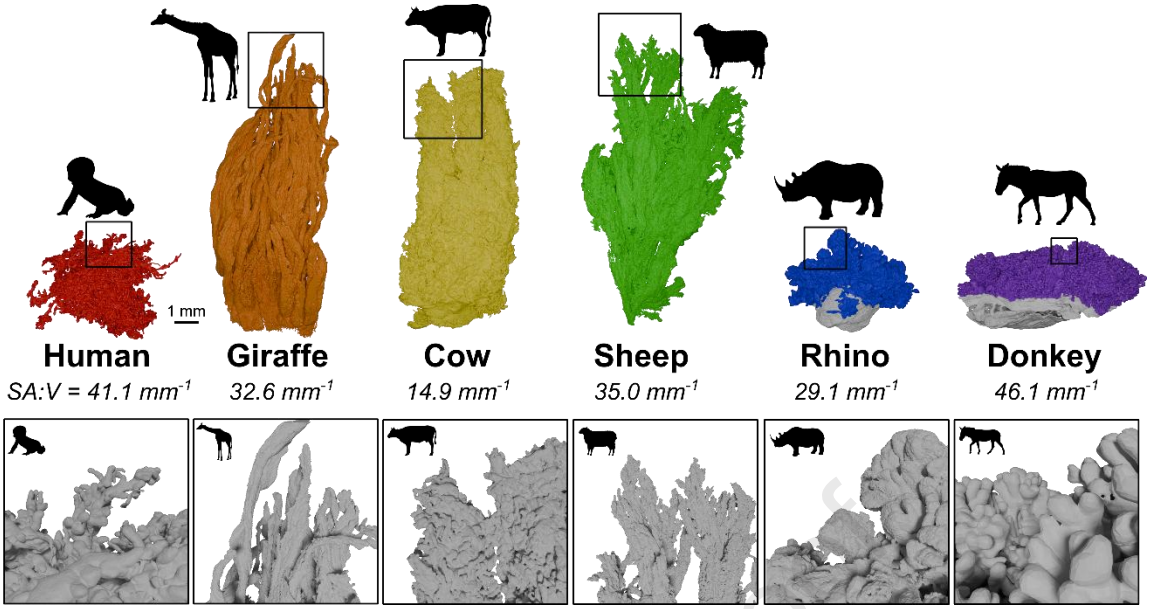

473

474 **Figure 5 – 3D imaging allows systematic interspecific comparison of villous**
475 **morphology.** Samples of placental villous tissue from different mammal species 3D
476 imaged by CXEM microCT. Reconstructions are shown to scale (top) with quantitative
477 metrics (surface area: volume ratio (SA:V)) and square insets magnified (bottom) for
478 comparison of qualitative villous morphology. SA:V values are for individual tissue
479 pieces only and are not meant to imply broad interspecific differences without further
480 replication.

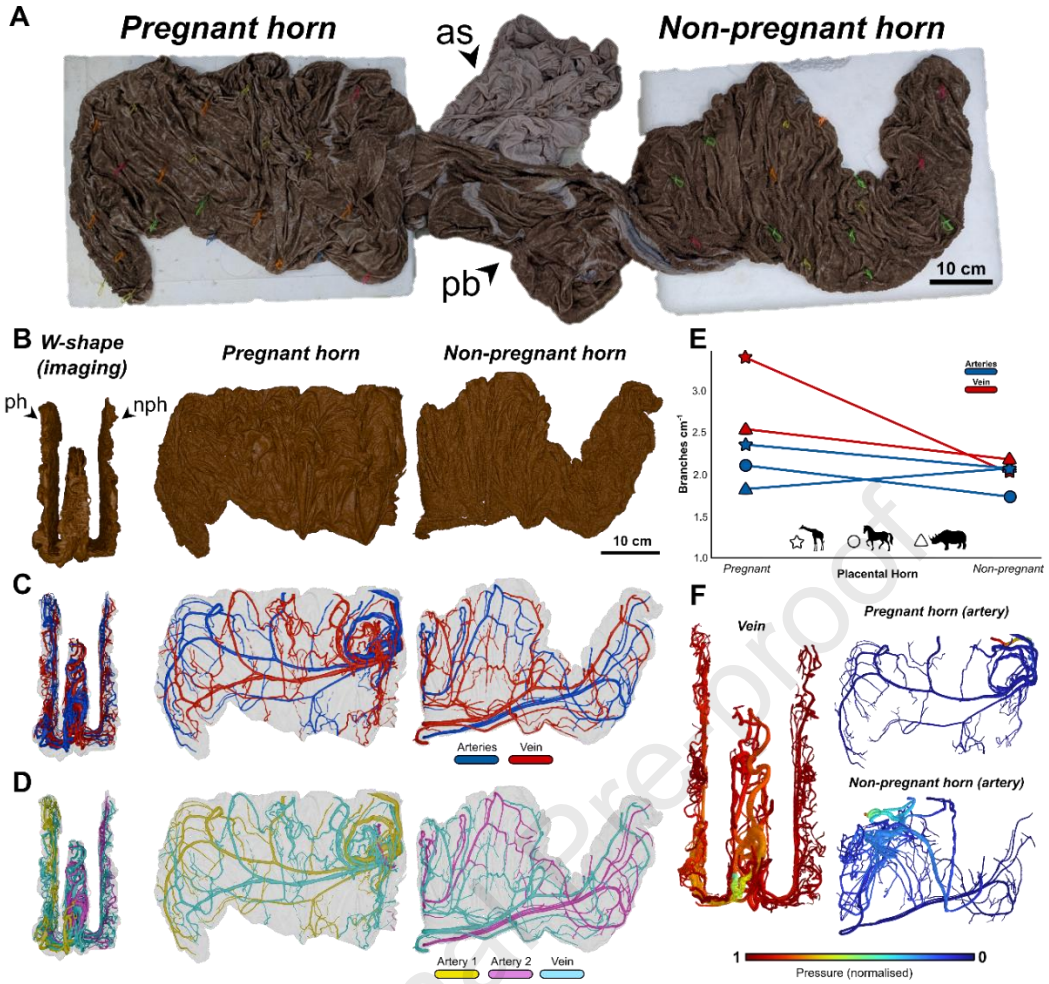

Figure 6 - Blood vessel analysis from a whole rhino placenta. (A) An entire rhino placenta was mounted to polystyrene boards and imaged using the walk-in d5 microCT system described above. Coloured plastic toothpicks hold the tissue in place. As = amniotic sac, pb = placental body. (B-D) The 3D reconstructed microCT scan (B) permitted full quantitative analysis of the rhino placental vasculature for both venous and arterial portions (C) and individual vessels (D). Skeletonization analysis shows blood vessels are generally more branched in the pregnant horn than the non-pregnant horn for our imaged large mammal placentas (E), but further biological replication is needed to confirm these preliminary trends. 3D reconstructed vasculature from the whole imaged rhino placenta is used as realistic tissue architecture in which to model blood flow in individual vessels, showing higher resistance in the pregnant horn artery than the non-pregnant horn artery (F). Note the pressure gradient in the vein is reversed compared to the artery, with flow from peripheral veins to the central vein.

References

[1] D. Laundon, N.J. Gostling, B.G. Sengers, P. Chavatte-Palmer, R.M. Lewis, Placental evolution from a three-dimensional and multiscale structural perspective, Evolution 78 (2023) 13-25.

[2] G.J. Burton, Placental Types, Benirschke's Pathology of the Human Placenta, Springer Nature, Switzerland, (2022) 23-38.

[3] A.M. Carter, Genomics, the diversification of mammals, and the evolution of placentation, Dev Biol 516 (2024) 167-182.

[4] S. Furukawa, Y. Kuroda, A. Sugiyama, A Comparison of the Histological Structure of the Placenta in Experimental Animals, J Toxicol Pathol 27(1) (2014) 11-18.

[5] D. Laundon, N. Gostling, B. Sengers, P. Chavatte-Palmer, R. Lewis, Comparative Placentation from a Three-Dimensional and Multiscale Structural Perspective, Placenta 140 (2023) E9-E10.

[6] A. Edu, C. Teodorescu, C.G. Dobjanschi, Z.Z. Socol, V. Teodorescu, A. Matei, D.F. Albu, G. Radulian, Placenta changes in pregnancy with gestational diabetes, Rom J Morphol Embryo 57(2) (2016) 507-512.

[7] E. Ehlers, O.O. Talton, D.J. Schust, L.C. Schulz, Placental structural abnormalities in gestational diabetes and when they develop: A scoping review, Placenta 116 (2021) 58-66.

[8] Y. Wubale, Tolera, A., Gross morphological study of placenta in preeclampsia, Anatomy Journal of Africa 6 (2017) 977-81.

[9] S. Kishwara, Ara, S., Rayhan, K.A., Begum, M. , Morphological changes of placenta in preeclampsia., Bangladesh Journal of Anatomy 7 (2009) 49-54.

[10] S. Biswas, S.K. Ghosh, Gross morphological changes of placentas associated with intrauterine growth restriction of fetuses: A case control study, Early Hum Dev 84(6) (2008) 357-362.

[11] S.M. Almasry, A.K. Elfayomy, Morphometric analysis of terminal villi and gross morphological changes in the placentae of term idiopathic intrauterine growth restriction, Tissue Cell 44(4) (2012) 214-219.

[12] M. Robles, P.M. Peugnet, S.A. Valentino, C. Dubois, M. Dahirel, M.C. Aubrière, F. Reigner, D. Serteyn, L. Wimel, A. Couturier-Tarrade, P. Chavatte-Palmer, Placental alterations in structure and function in intra-uterine growth-retarded horses, Equine Vet J 50(3) (2018) 405-414.

[13] M.M. Kamal, M. Van Eetvelde, L. Vandaele, G. Opsomer, Environmental and maternal factors associated with gross placental morphology in dairy cattle, Reprod Domest Anim 52(2) (2017) 251-256.

[14] F. Constant, M. Guillomot, Y. Heyman, X. Vignon, P. Laigre, J.L. Servely, J.P. Renard, P. Chavatte-Palmer, Large offspring or large placenta syndrome? Morphometric analysis of late gestation bovine placentomes from somatic nuclear transfer pregnancies complicated by hydrallantois, Biol Reprod 75(1) (2006) 122-130.

[15] S.F. Peek, Dropsical Conditions Affecting Pregnancy, Current Therapy in Large Animal Theriogenology (1997) 428-431.

[16] D. Laundon, E. Proudley, P.J. Basford, O.L. Katsamenis, D.S. Chatelet, J.K. Cleal, N.J. Gostling, P. Chavatte-Palmer, R.M. Lewis, Quantitative microCT imaging of a whole equine placenta and its blood vessel network, Placenta 154 (2024) 216-219.

[17] R. Leiser, P. Kaufmann, Placental Structure - in a Comparative Aspect, Exp Clin Endocrinol 102(3) (1994) 122-134.

[18] T.O. Junaid, P. Brownbill, N. Chalmers, E.D. Johnstone, J.D. Aplin, Fetoplacental vascular alterations associated with fetal growth restriction, Placenta 35(10) (2014) 808-815.

[19] X.Y. Shen, C.J. Wang, X.J. Yue, Q.J. Wang, L.J. Xie, Z.Q. Huang, X.W. Huang, J.Q. Li, Y. Xu, L. Chen, S. Lye, Y.X. Wei, Z.J. Wang, Preeclampsia associated changes in volume density of fetoplacental vessels in Chinese women and mouse model of preeclampsia, Placenta 121 (2022) 116-125.

[20] M. Pozor, Equine placenta–A clinician's perspective. Part 1: Normal placenta–Physiology and evaluation., Equine Veterinary Education 28 (2016) 327-334.

[21] S.G. Caspe, M. Livingstone, D. Frew, K. Aitchison, S.R. Wattegedera, G. Entrican, J. Palarea-Albaladejo, T.N. McNeilly, E. Milne, N.D. Sargison, F. Chianini, D. Longbottom, The 1B vaccine strain of produces placental pathology indistinguishable from a wild type infection, Plos One 15(11) (2020) p.e0242526.

[22] R.M. Lewis, Volume electron microscopy reveals placental ultrastructure in 3D, Placenta (2023) 78-83.

[23] R.M. Lewis, J.E. Pearson-Farr, Multiscale three-dimensional imaging of the placenta, Placenta 102 (2020) 55-60.
[24] D. Laundon, O.L. Katsamenis, J. Thompson, P. Goggin, D.S. Chatelet, P. Chavatte-Palmer, N.J. Gostling, R.M. Lewis, Correlative multiscale microCT-SBF-SEM imaging of resin-embedded tissue, Methods in Cell Biology, Academic Press (2023) 241-267.
[25] D. Laundon, B.G. Sengers, J. Thompson, S.E. Harris, O. Beasley, P.J. Basford, O.L. Katsamenis, P. Goggin, E. Derisoud, D. Fanelli, C. Bocci, F. Camillo, J. Shotton, G. Constable-Dakeyne, N.J. Gostling, P. Chavatte-Palmer, R.M. Lewis, Convergently evolved placental villi show multiscale structural adaptations to differential placental invasiveness, Biol Letters 20(3) (2024) p.20240016.
[26] D. Laundon, T. Lane, O. Katsamenis, J. Norman, L. Brewer, S. Harris, P. Basford, J. Shotton, D. Free, G. Constable-Dakeyne, N. Gostling, P. Chavatte-Palmer, R. Lewis, Correlative Three-Dimensional X-Ray Histology (3D-XRH) as a Tool for Quantifying Mammalian Placental Structure, Placenta 154 (2024) E11-E11.
[27] S. Savatovic, D. Laundon, F. De Marco, M. Riedel, J.U. Hammel, M. Busse, M. Salome, L. Pascolo, I. Zanette, R.M. Lewis, J. Herzen, P. Thibault, High-resolution X-ray phase-contrast tomography of human placenta with different wavefront markers, Sci Rep-Uk 15(1) (2025) 2131.
[28] R.M. Lewis, H. Baskaran, J. Green, S. Tashev, E. Palaiologou, E.M. Lofthouse, J.K. Cleal, A. Page, D.S. Chatelet, P. Goggin, B.G. Sengers, 3D visualization of trans-syncytial nanopores provides a pathway for paracellular diffusion across the human placental syncytiotrophoblast, iScience 25(12) (2022) 105453.
[29] N. Scher, O. Avinoam, 50 Shades of CLEM: How to choose the right approach for you, Correlative Light and Electron Microscopy 162 (2021) 1-11.
[30] V. Dantzer, Leiser, R., Kaufmann, P., Luckhardt, M., Comparative morphological aspects of placental vascularization., Placental Vascularization and Blood Flow: Basic Research and Clinical Applications (1988) 235-260.
[31] C.E. Hayward, S. Lean, C.P. Sibley, R.L. Jones, M. Wareing, S.L. Greenwood, M.R. Dilworth, Placental Adaptation: What Can We Learn from Birthweight:Placental Weight Ratio?, Front Physiol 7 (2016) 28.
[32] Y. Matsuda, T. Itoh, H. Itoh, M. Ogawa, K. Sasaki, N. Kanayama, S. Matsubara, Impact of placental weight and fetal/placental weight ratio Z score on fetal growth and the perinatal outcome, Int J Med Sci 15(5) (2018) 484-491.
[33] H. Azpurua, E.F. Funai, L.M. Coraluzzi, L.F. Doherty, I.E. Sasson, M. Kliman, H.J. Kliman, Determination of Placental Weight Using Two-dimensional Sonography and Volumetric Mathematic Modeling, Am J Perinat 27(2) (2010) 151-155.
[34] L.E. Higgins, L. Simcox, C.P. Sibley, A.E.P. Heazell, E.D. Johnstone, Third trimester placental volume and biometry measurement: A method-development study, Placenta 42 (2016) 51-58.
[35] C.M. Salafia, M. Yampolsky, D.P. Misra, O. Shlakhter, D. Haas, B. Eucker, J. Thorp, Placental surface shape, function, and effects of maternal and fetal vascular pathology, Placenta 31(11) (2010) 958-962.
[36] Y.J. Lee, Mi-Young L., Chung, J.H., Won, H.S., Park, B., Birth weight prediction using artificial intelligence-based placental assessment from macroscopic photo: a retrospective study., Placenta (2025) 23.
[37] A.M. Abdalla, M.D. Tingari, M.A. Abdalla, Histomorphometric parameters of normal full term placenta of Sudanese women, Heliyon 2(7) (2016) e00135.
[38] E.M. Laga, S.G. Driscoll, H.N. Munro, Quantitative Studies of Human Placenta .2. Biochemical Characteristics, Biol Neonate 23(3-4) (1973) 260-283.
[39] M.K. John, Ranjith, S., Sampson, U., Fysal, N., Ansari, A.W., TL, J., Correlation of placental morphometry with birth weight and gestational age., Scholars Int J Anat Physiol 2 (2019) 318-24.
[40] M.C. Veronesi, M. Villani, S. Wilsher, A. Contri, A. Carluccio, A comparative stereological study of the term placenta in the donkey, pony and Thoroughbred, Theriogenology 74(4) (2010) 627-631.
[41] N. Schwartz, I. Oguz, J.C. Wang, A. Pouch, N. Yushkevich, S. Parameshwaran, J. Gee, P. Yushkevich, B. Oguz, Fully Automated Placental Volume Quantification From 3D Ultrasound for Prediction of Small-for-Gestational-Age Infants, Obstet Gynecol Surv 77(12) (2022) 713-715.
[42] T. Hata, H. Tanaka, J. Noguchi, K. Hata, Three-dimensional ultrasound evaluation of the placenta, Placenta 32(2) (2011) 105-115.
[43] E. Lecarpentier, O. Morel, A. Tarrade, M. Dahirel, M. Bonneau, E. Gayat, D. Evain-Brion, P. Chavatte-Palmer, V. Tsatsaris, Quantification of utero-placental vascularization in a rabbit model three-dimensional power Doppler angiography, Placenta 33(10) (2012) 769-775.

[44] O. Morel, F. Pachy, P. Chavatte-Palmer, M. Bonneau, E. Gayat, P. Laigre, D. Evain-Brion, V. Tsatsaris, Correlation between uteroplacental three-dimensional power Doppler indices and true uterine blood flow: evaluation in a pregnant sheep model, Ultrasound Obst Gyn 36(5) (2010) 635-640.
[45] D. Flouri, J.R.T. Darby, S.L. Holman, S.R. Perumal, A.L. David, J.L. Morrison, A. Melbourne, Magnetic resonance imaging of placentome development in the pregnant Ewe, Placenta 105 (2021) 61-69.
[46] M. Dap, T. Albert, I. Ramdhani, A. Couturier-Tarrade, O. Morel, P. Chavatte-Palmer, M. Beaumont, C. Bertholdt, Is the rabbit a natural model of fetal growth restriction? Morphological and functional characterization study using diffusion-weighted MRI and stereology, Placenta 154 (2024) 74-79.
[47] K. De Clercq, E. Persoons, T. Napso, C. Luyten, T.N. Parac-Vogt, A.N. Sferruzzi-Perri, G. Kerckhofs, J. Vriens, High-resolution contrast-enhanced microCT reveals the true three-dimensional morphology of the murine placenta, P Natl Acad Sci USA 116(28) (2019) 13927-13936.
[48] S. Perazzolo, R.M. Lewis, B.G. Sengers, Modelling the effect of intervillous flow on solute transfer based on 3D imaging of the human placental microstructure, Placenta 60 (2017) 21-27.
[49] R.P. Mayo, Y. Abbas, D.S. Charnock-Jones, G.J. Burton, G. Marom, Three-dimensional morphological analysis of placental terminal villi, Interface Focus 9(5) (2019) 20190037.
[50] U.H. Wagner, C. Rau, Optical Design in Phase-Space for the I13L X-Ray Imaging and Coherence Beamline at Diamond using XPHASY, Aip Conf Proc 1234 (2010) 461-464.
[51] K.A. Staines, S. Parker, B. Poulet, S. Mirczuk, R.C. Fowkes, M. Hopkinson, K. Madi, P.D. Lee, A.A. Pitsillides, Str/Ort Mice Exhibit an Inherent Endochondral Growth Defect and Redeploy Transient Chondrocyte Behaviours Prior to Osteoarthritis Onset, Osteoarthr Cartilage 22 (2014) S357-S357.
[52] W.M. Tun, G. Poologasundarampillai, H. Bischof, G. Nye, O.N.F. King, M. Basham, Y. Tokudome, R.M. Lewis, E.D. Johnstone, P. Brownbill, M. Darrow, I.L. Chernyavsky, A massively multi-scale approach to characterizing tissue architecture by synchrotron micro-CT applied to the human placenta, J R Soc Interface 18(179) (2021) 20210140.
[53] C.L. Walsh, P. Tafforeau, W.L. Wagner, D.J. Jafree, A. Bellier, C. Werlein, M.P. Khnel, E. Boller, S. Walker-Samuel, J.L. Robertus, D.A. Long, J. Jacob, S. Marussi, E. Brown, N. Holroyd, D.D. Jonigk, M. Ackermann, P.D. Lee, Imaging intact human organs with local resolution of cellular structures using hierarchical phase-contrast tomography, Nat Methods 18(12) (2021) 1532.
[54] J. Reichmann, A. Schnurpfeil, S. Mittelstaedt, P.M. Jensen, V.A. Dahl, A.B. Dahl, C. Weide, E. von Campenhausen, H. Dejea, P. Tafforeau, C. Werlein, D. Jonigk, M. Ackermann, K. Engel, J. Gallwas, A. Dietz, M.F. Hasanov, T. Salditt, 3D multiscale characterization of the human placenta: Bridging anatomy and histology by X-ray phase-contrast tomography, PNAS Nexus 4(1) (2025) pgae583.
[55] D.J.P. Barker, K.L. Thornburg, C. Osmond, E. Kajantie, J.G. Eriksson, The surface area of the placenta and hypertension in the offspring in later life, Int J Dev Biol 54(2-3) (2010) 525-530.
[56] L. Sletner, C.S. Yajnik, G. Turowski, T.M. Michelsen, C. Sommer, K.I. Birkeland, B. Roald, A.K. Jenum, Placental weight, surface area, shape and thickness- Relations with maternal ethnicity and cardio-metabolic factors during pregnancy, Placenta 148 (2024) 69-76.
[57] M. Yampolsky, C.M. Salafia, O. Shlakhter, D. Haas, B. Eucker, J. Thorp, Modeling the variability of shapes of a human placenta, Placenta 29(9) (2008) 790-797.
[58] P. Rana, S.K. Razdan, S. Kumar, Morphometric study of human placenta and an insight into its vascular pattern by corrosion cast technique, Indian Journal of Clinical Anatomy and Physiology 8 (2018) 123-9.
[59] M. Robles, P.M. Peugnet, S.A. Valentino, C. Dubois, M. Dahirel, M.C. Aubrière, F. Reigner, D. Serteyn, L. Wimel, A. Tarrade, P. Chavatte-Palmer, Placental structure and function in different breeds in horses, Theriogenology 108 (2018) 136-145.
[60] A. Kazemian, R. Hooshmandabbasi, E.M. Schraner, A. Boos, K. Klisch, Evolutionary implications of fetal and maternal microvillous surfaces in epitheliochorial placentae, J Morphol 280(4) (2019) 615-622.
[61] T.M. Mayhew, Stereology and the placenta: Where's the point? A review, Placenta 27 (2006) S17-S25.
[62] T.M. Mayhew, G.J. Burton, Stereology and Its Impact on Our Understanding of Human Placental Functional Morphology, Microsc Res Techniq 38 (1997) 195-205.
[63] S.M. Nelson, P.M. Coan, G.J. Burton, R.S. Lindsay, Placental Structure in Type 1 Diabetes Relation to Fetal Insulin, Leptin, and IGF-I, Diabetes 58(11) (2009) 2634-2641.
[64] E. Haeussner, B. Aschauer, G.J. Burton, B. Huppertz, F.E. von Koch, J. Muller-Starck, C. Salafia, C. Schmitz, H.G. Frank, Does 2D-Histologic identification of villous types of human placentas at birth enable sensitive and reliable interpretation of 3D structure?, Placenta 36(12) (2015) 1425-1432.

[65] K. De Clercq, J. Lopez-Tello, J. Vriens, A.N. Sferruzzi-Perri, Double-label immunohistochemistry to assess labyrinth structure of the mouse placenta with stereology, Placenta 94 (2020) 44-47.
[66] A.L. Karimu, G.J. Burton, The distribution of microvilli over the villous surface of the normal human term placenta is homogenous, Reprod Fert Develop 7(5) (1995) 1269-1273.
[67] S.E. Harris, K.S. Matthews, E. Palaiologou, S.A. Tashev, E.M. Lofthouse, J. Pearson-Farr, P. Goggin, D.S. Chatelet, D.A. Johnston, M.S. Jongen, A.M. Page, J.K. Cleal, R.M. Lewis, Pericytes on placental capillaries in terminal villi preferentially cover endothelial junctions in regions furthest away from the trophoblast, Placenta 104 (2021) 1-7.
[68] S.A. Tashev, D. Parsons, C. Hillman, S. Harris, E.M. Lofthouse, P. Goggin, D.S. Chatelet, J.K. Cleal, N. Smyth, H. Palaiologou, A. Page, R.M. Lewis, Folding of the syncytiotrophoblast basal plasma membrane increases the surface area available for exchange in human placenta, Placenta 117 (2022) 57-63.
[69] E. Palaiologou, P. Goggin, D.S. Chatelet, R.R. de Souza, W. Chiu, B. Ashley, E.M. Lofthouse, B.G. Sengers, C. Torrens, A.M. Page, J.K. Cleal, R.M. Lewis, Serial block-face scanning electron microscopy reveals novel intercellular connections in human term placental microvasculature, J Anat 237(2) (2020) 241-249.
[70] P.M. Coan, A.C. Ferguson-Smith, G.J. Burton, Developmental dynamics of the definitive mouse placenta assessed by stereology, Biol Reprod 70(6) (2004) 1806-1813.
[71] R. Baur, Morphometry of the placental exchange area, Adv Anat Embryol Cell Biol. 53 (1977) 3-65.
[72] B. Albl, S. Haesner, C. Braun-Reichhart, E. Streckel, S. Renner, F. Seeliger, E. Wolf, R. Wanke, A. Blutke, Tissue Sampling Guides for Porcine Biomedical Models, Toxicol Pathol 44(3) (2016) 414-420.
[73] E. Haeussner, A. Buehlmeyer, C. Schmitz, F.E. von Koch, H.G. Frank, Novel 3D Microscopic Analysis of Human Placental Villous Trees Reveals Unexpected Significance of Branching Angles, Sci Rep-Uk 4 (2014) 6192.
[74] J.L. James, Y. Tongpob, V. Srinivasan, R.C. Crew, N. Bappoo, B. Doyle, D. Gerneke, A.R. Clark, C.S. Wyrwoll, Three-dimensional visualisation of the feto-placental vasculature in humans and rodents, Placenta 114 (2021) 8-13.
[75] T.O. Junaid, R.S. Bradley, R.M. Lewis, J.D. Aplin, E.D. Johnstone, Whole organ vascular casting and microCT examination of the human placental vascular tree reveals novel alterations associated with pregnancy disease, Sci Rep-Uk 7 (2017) 4144.
[76] T. Wan, D. Laundon, S.N. Saw, N. Cheng, H.K. Lee, E.D. Johnstone, O.E. Jensen, R.M. Lewis, I.L. Chernyavsky, Umbilical cord structure shapes feto-maternal heat exchange across mammals, biorxiv (2025) 2025.11.18.688874.
[77] R.G. Shah, C.M. Salafia, T. Girardi, L. Conrad, K. Keaty, A. Bartleotc, Shape matching algorithm to validate the tracing protocol of placental chorionic surface vessel networks, Placenta 36(8) (2015) 944-946.
[78] D.L. Bergman, U. Ullberg, Scaling properties of the placenta's arterial tree, J Theor Biol 193(4) (1998) 731-738.
[79] D. Laundon, N. Chrismas, G. Wheeler, M. Cunliffe, Chytrid rhizoid morphogenesis resembles hyphal development in multicellular fungi and is adaptive to resource availability, P Roy Soc B-Biol Sci 287 (2020) p.20200433.
[80] T.M. Mayhew, Stereological studies on fetal vascular development in human placental villi., Image Analysis and Stereology 22 (2003) 49-56.
[81] I. Couck, M. Aertsen, A. Jespers, S. Deneckere, L. Lewi, The assessment of placental sharing using X-ray angiogram versus digital photograph: A prospective study, Placenta 83 (2019) 1-4.
[82] E.N. Gomez, T.M. Ahmed, K. Macura, E.K. Fishman, A.J. Vaught, CT angiography for characterization of advanced placenta accreta spectrum: indications, risks, and benefits, Abdom Radiol 49(3) (2024) 842-854.
[83] L.T. Mercé, M.J. Barco, J.L. Alcázar, R. Sabatel, J. Troyano, Intervillous and uteroplacental circulation in normal early pregnancy and early pregnancy loss assessed by 3-dimensional power Doppler angiography, Am J Obstet Gynecol 200(3) (2009) 315-e1.
[84] Y. Tongpob, S.S. Xia, C. Wyrwoll, A. Mehnert, Quantitative characterization of rodent feto-placental vasculature morphology in micro-computed tomography images, Comput Meth Prog Bio 179 (2019) 104984.
[85] C.L. Fonta, B.M. Humbel, Correlative microscopy, Arch Biochem Biophys 581 (2015) 98-110.
[86] K. Anderson, T. Nilsson, J. Fernandez-Rodriguez, Challenges for CLEM from a light microscopy perspective., in: P. Verkade, L.M. Collinson (Eds.), Correlative Imaging: Focusing on the Future, John Wiley & Sons Ltd (2019) 23-35.

[87] O.L. Katsamenis, M. Olding, J.A. Warner, D.S. Chatelett, M.G. Jones, G. Sgalla, B. Smit, O.J. Larkin, I. Haig, L. Richeldi, I. Sinclair, P.M. Lackie, P. Schneider, X-ray Micro-Computed Tomography for Nondestructive Three-Dimensional (3D) X-ray Histology, Am J Pathol 189(8) (2019) 1608-1620.
[88] O.L. Katsamenis, P.J. Basford, S.K. Robinson, R.P. Boardman, E. Konstantinopoulou, P.M. Lackie, A. Page, J.A. Ratnayaka, P. Goggin, G.J. Thomas, S.J. Cox, I. Sinclair, P. Schneider, A high-throughput 3D X-ray histology facility for biomedical research and preclinical applications, Wellcome Open Res 8 (2023) 366.
[89] S.A. Elmore, R.Z. Cochran, B. Bolon, Histology Atlas of the Developing Mouse Placenta, Toxicol Pathol 50 (1) (2023) 60-117.
[90] I. Belevich, M. Joensuu, D. Kumar, H. Vihinen, E. Jokitalo, Microscopy Image Browser: A Platform for Segmentation and Analysis of Multidimensional Datasets, Plos Biol 14(1) (2016).
[91] J.M. Lucocq, T.M. Mayhew, Y. Schwab, A.M. Steyer, C. Hacker, systems biology in 3D space - enter the morphome, Trends Cell Biol 25(2) (2015) 59-64.
[92] T.M. Mayhew, Morphomics: An integral part of systems biology of the human placenta, Placenta 36(4) (2015) 329-340.
[93] F. Deeba, R.C.Y. Hu, V. Lessoway, J. Terry, D. Pugash, C. Mayer, J. Hutcheon, S. Salcudean, R. Rohling, Project SWAVE 2.0: An overview of the study design for multimodal placental image acquisition and alignment, Methodsx 9 (2022) p.101738.
[94] J.D.B. O'Sullivan, S.M. Cruickshank, T. Starborg, P.J. Withers, K.J. Else, Characterisation of cuticular inflation development and ultrastructure in *Trichuris muris* using correlative X-ray computed tomography and electron microscopy, Sci Rep-Uk 10(1) (2020) 5846.
[95] T. Starborg, J.D.B. O'Sullivan, C.M. Carneiro, J. Behnsen, K.J. Else, R.K. Grencis, P.J. Withers, Experimental steering of electron microscopy studies using prior X-ray computed tomography, Ultramicroscopy 201 (2019) 58-67.
[96] P. Parlanti, V. Cappello, F. Brun, G. Tromba, R. Rigolio, I. Tonazzini, M. Cecchini, V. Piazza, M. Gemmi, Size and specimen-dependent strategy for X-ray micro-ct and tem correlative analysis of nervous system samples, Sci Rep-Uk 7 (2017) 2858.
[97] T. Deerinck, E. Bushong, X. Shu, R. Tsien, M. Ellisman, Enhancing serial block-face scanning electron microscopy to enable high resolution 3-D nanohistology of cells and tissues., Microscopy and Microanalys 16 (2010) 1138-9.
[98] W. Denk, H. Horstmann, Serial block-face scanning electron microscopy to reconstruct three-dimensional tissue nanostructure, Plos Biol 2(11) (2004) 1900-1909.
[99] G.J. Burton, E. Jauniaux, Sonographic, Stereological and Doppler Flow Velocimetric Assessments of Placental Maturity, Brit J Obstet Gynaec 102(10) (1995) 818-825.
[100] S. Wilsher, F. Stansfield, R.E.S. Greenwood, P.D. Trethowan, R.A. Anderson, F.B.W. Wooding, W.R. Allen, Ovarian and placental morphology and endocrine functions in the pregnant giraffe (*Giraffa camelopardalis*), Reproduction 145(6) (2013) 541-554.

CONFLICT OF INTEREST STATEMENT

We declare we have no competing interests.